NJC

PAPER

Cite this: *New J. Chem.*, 2015, **39**, 8887

The impact of the polar core size and external organic media composition on micelle–micelle interactions: the effect on gold nanoparticle synthesis

Jorge A. Gutierrez,* M. Alejandra Luna, N. Mariano Correa, Juana J. Silber and R. Darío Falcone*

Received (in Nottingham, UK) 5th May 2015,
Accepted 3rd September 2015

DOI: 10.1039/c5nj01126d

www.rsc.org/njc

We report the effect of the molar ratio parameter W_0 (W_0 = [water]/[surfactant]) and the external organic media composition on benzyl-*n*-hexadecyldimethylammonium chloride (BHDC) reverse micelle (RM) interactions, the key step to nanoparticle synthesis using RMs as nanoreactors. The results show a better interaction between BHDC RM droplets when the external media contain toluene:hexane blends instead of pure toluene. This organic solvent mixture enhances the material exchange between droplets and more well defined and smaller gold nanoparticles were obtained at the two W_0 studied (3 and 6). On the other hand, BHDC RMs created in pure toluene give a stiffer environment with poor droplet–droplet interaction, and the Cl^- counterions affect the growth of the particles, leading to different morphologies and sub-nanometer gold species production. These results are very promising for many applications. This work shows how each RM system is a unique and tunable nanoreactor.

Introduction

One of the most important areas of soft matter that gains attention from different fields of academia and industry of materials is the production of nanocomposites.[1] Among all compounds involved in nanotechnology, metal nanoparticles (NPs) are one of the most important composites, being ubiquitous as basic components in many products.[2] There are many metal NPs nowadays being used in different applications, however gold NPs (AuNPs) stand out because they have numerous physical, chemical and biological properties triggered by small changes in their nanometric size and morphology.[3] AuNPs can be easily functionalized with a variety of compounds such as antibodies, polymers, molecular probes, drugs, and genetic materials.[4,5] Furthermore, AuNPs are distinguished for their nontoxic properties in smart delivery systems linked to internal or external stimulation,[6,7] being important materials for nanobiotechnology and nanomedicine.[4,8] Several parameters are able to modify the growth and size of AuNPs, among them are: synthetic methodology, reducing agents, the reduction rate and temperature, the concentration of precursors, *etc.*[9,10] One of the most versatile methods implemented in NP synthesis is the use of reverse micelles (RMs) as nanoreactors, allowing the formation of different nanocompounds by just changing one variable (the organic phase, surfactant or polar solvent content).[11,12] RMs are supramolecular assemblies formed when surfactants are dissolved in nonpolar organic solvents, their polar area being located in the interior (core), while their hydrocarbon tails extend into the nonpolar medium (see Fig. 1).[13] RMs have practical importance in different areas such as detergents, foodstuffs, and cosmetics, and have been evaluated as unique and versatile media for a variety of chemical or biochemical reactions.[14] Most of the phenomena and properties of RMs have their origin in the droplet–droplet interaction, thus, the composition of RMs is a fundamental fact that impacts the droplet size, the fluidity of the interface, and the interaction between droplets.[15,16] Lemaire *et al.*[17] proposed that attractive droplet–droplet interaction depends on the mutual interpenetration of the surfactant tails over some small distance without

Departamento de Química, Universidad Nacional de Río Cuarto, Agencia Postal # 3, C.P. X5804BYA, Río Cuarto, Argentina. E-mail: jgutierrez@exa.unrc.edu.ar, rfalcone@exa.unrc.edu.ar

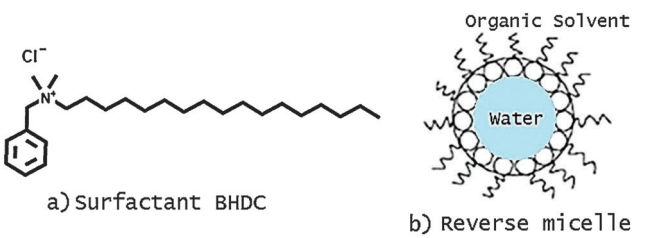

Fig. 1 (a) Representation of the cationic surfactant BHDC and (b) schematic representation of an aqueous reverse micelle.

much entropy loss and a decrease in the total free energy of the system. This is possible because the surfactant tail–tail interactions are not much stronger than the surfactant–nonpolar external solvent interactions, thus, many properties of RMs can be modified by changes in the composition of the nonpolar solvent.[18–23] Perhaps one of the most important properties of RMs is their ability to dissolve polar solvents in the inner polar pool. This property allows the synthesis of NPs using the polar pool as a nanoreactor.[11] A variety of anionic, cationic and nonionic surfactants have been employed to prepare RMs.[13,22,24] In this way, their versatility and properties strongly depend on different conditions such as the chemical properties of the surfactant, the external nonpolar solvent and the polar solvent inside.[13] Among the anionic surfactants that form RMs, the best known are those systems assembled from sodium 1,4-bis-2-ethylhexylsulfosuccinate (AOT) in different nonpolar solvents.[13] Indeed, in NP synthesis it is common to find studies in RMs employing anionic[25] and non-ionic surfactants.[26] However, to our knowledge, there are no studies using benzyl-*n*-hexadecyldimethylammonium chloride (BHDC, see Fig. 1) as a cationic surfactant in NP synthesis despite that BHDC is distinguished because, unlike other cationic surfactants, it readily forms RMs without co-surfactant addition[23,27] and our group has found recent interesting results about their modulated properties such as micellar interactions, and size and interfacial micropolarity,[23,28] that allow us to understand the nature of the RM interface before using it as a nanoreactor in NP synthesis. Also, we used the very well-known gold NPs in order to perform such an investigation, for the first time, in an unknown RM medium such as BHDC RMs.

Moreover, as the NP synthesis is based on Brownian motion and interactions between droplets that form fused dimers (or encounter pairs) in which the reactants are exchanged, we hypothesize that by changing the external solvent composition and the polar core, different NPs can be obtained. In this sense it could be possible to make tunable nanoreactors for metal NP synthesis. Herein, we report the strong dependence on the water content W_0 (W_0 = [water]/[BHDC]) and the organic medium composition (toluene:hexane blend) that cationic BHDC RMs have on the growth, size, concentration, morphology and spectroscopic properties of AuNPs synthesized inside these nanoreactors.

Results and discussion

AuNPs in toluene/BHDC/water RMs

As a first step in the synthesis of AuNPs we determine the apparent hydrodynamic diameter (d_{app}) of toluene/BHDC/water RMs by DLS in the absence of reactants (tetrachloroauric acid and hydrazine) at two W_0 values: 3 and 6.

Our results show droplets with a d_{app} value of 3.5 ± 0.5 nm at W_0 = 3 and 4.6 ± 0.5 nm at W_0 = 6. These values are consistent with the d_{app} values reported before for similar BHDC RMs.[22] Once the sizes of the nanoreactors were determined, we proceeded to dissolve the reactants (tetrachloroauric acid and hydrazine) into the polar core in order to form AuNPs using the methodology described by Lopez-Quintela.[11] The reactants

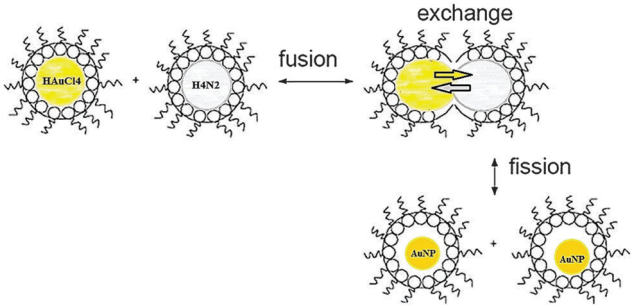

Fig. 2 Schematic representation of interdroplet interactions between two RMs.

interact inside the RMs and the auric ions are reduced in a confined environment, the polar core and, thus the nucleation and the nanoparticle growth is limited to a nanoscale space. This methodology is based on the Brownian motion of RMs and on droplet–droplet interactions forming a fused dimer (or an encounter pair) allowing the exchange of the reactants. Thus, if the precursors are dissolved inside the polar core, the reaction takes place at the nanoscale (Fig. 2).[11,29]

In order to evaluate the effect of polar core size on the NP growth and morphology, the gold reduction reaction was performed at two W_0 values (6 and 3). The reactants in the aqueous phase of BHDC RMs were incorporated as described in the Experimental section.

Fig. 3A shows the kinetic formation of the localized surface plasmon resonance (LSPR) for AuNPs synthesized in BHDC RMs at W_0 = 6.

The common situation in LSPR formation is the appearance of a unique band which increases its intensity as particles grow,[30] however our results (Fig. 3A) show the presence of two absorption maxima (λ_{max} = 537 and 630 nm). Interestingly, when the time of reaction increases, the intensity of the lower energy band decreases and, finally after 90 seconds the spectrum remains constant with a high energy band centered at λ_{max} = 537 nm and a small shoulder at lower energy. The electron micrograph obtained for the final reaction products (Fig. 3B) shows ellipsoidal morphologies of 25 ± 3 nm of size. As it is well known, the ellipsoidal shapes have two diameters (longitudinal and transversal) which give different plasmon resonances and would be an explanation for the shoulder shown in Fig. 3A. On the other hand, the size distribution shown in Fig. 3C is based on Mie theory and the Brownian motion of particles in solution, thus the particles disperse light in different positions expressed as a broad distribution, suggesting that the species are well dispersed in the medium, as it was observed in other systems.[31,32] Taking into account the form evolution of LSPRs, these results suggest that the particles are formed with an ellipsoidal morphology and become more spherical with reaction time. Furthermore, the colloidal AuNP solutions at 90 seconds of reaction show fluorescence emission properties as can be seen in Fig. 4, characteristic of sub-nanometer atom clusters.[29,33] It is important to note that the fluorescence emission of the precursors (tetrachloroauric acid and hydrazine

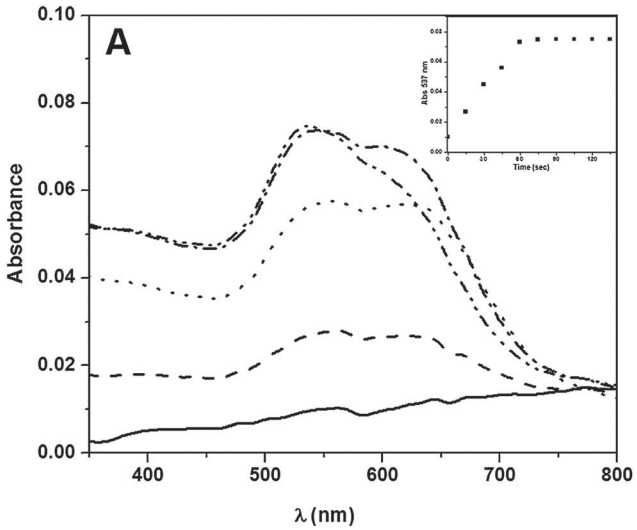

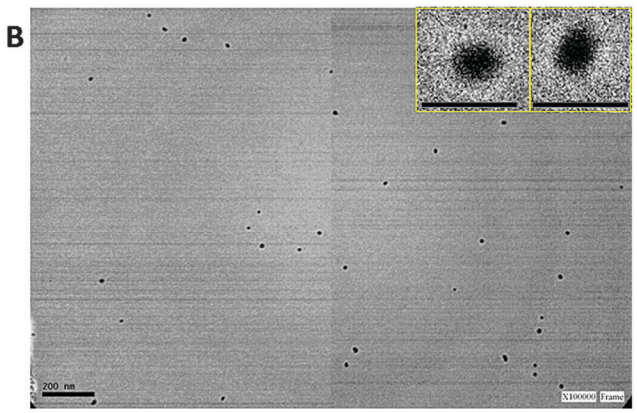

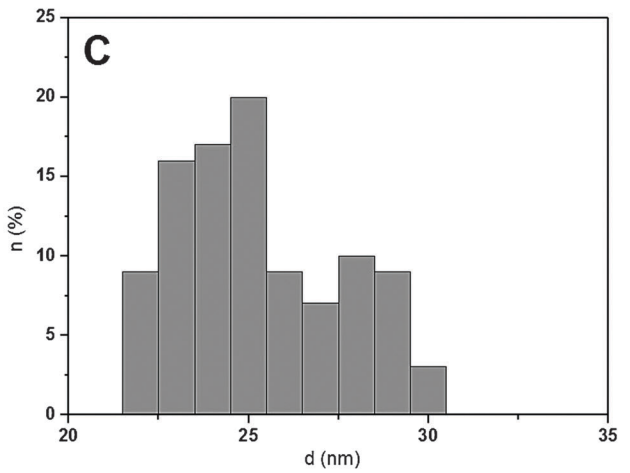

Fig. 3 (A) Absorption spectra during AuNP formation in toluene/BHDC/water at W_0 = 6. Time (s) = 0 (—), 15 (- - -), 45 (●●●), 60 (-·-) and 90 (–●●–). The inset in the top-right corresponds to the absorbance at λ = 537 nm *vs.* time (s). Aqueous BHDC RM solution (without precursors) was used as blank. (B) TEM micrographs of AuNPs synthesized in toluene/BHDC/water RMs at the end of the reaction (90 s). [BHDC] = 0.05 M, [$HAuCl_4$] = 0.005 M, [H_4N_2] = 0.3 M, W_0 = 6. Reference bar = 200 nm. The inset in the top-right corner corresponds to a zoom-in of two AuNPs, and the reference bar to 50 nm, and (C) size distribution by number at the end of the reaction (90 s).

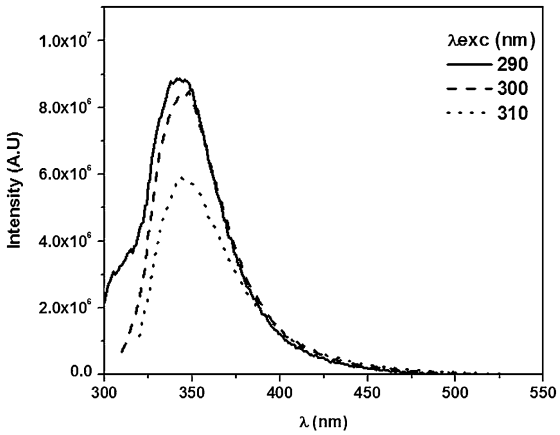

Fig. 4 Emission spectra of sub-nanometer gold particles synthesized in toluene/BHDC/water RMs varying the excitation wavelength. [BHDC] = 0.05 M, [$HAuCl_4$] = 0.005 M, [H_4N_2] = 0.3 M, W_0 = 6. Spectra taken at the end of the reaction (90 s).

RMs solutions) and the non-polar solvents was checked and discarded. In this sense, because of the absence of fluorescence in AuNPs $>$ 10 nm of diameter, the emission phenomenon is only a result of the presence of atomic clusters and not due to the enhancement of the precursor's emission by the presence of AuNPs in the media. Unfortunately, the sizes of the atomic clusters are below the resolution allowed by our TEM and cannot be observed in detail.

Fig. 4 shows the fluorescence emission spectra of the sub-nanometer gold particles formed in BHDC RMs excited at different wavelengths.

As can be seen in Fig. 4, the emission spectra show different intensities when the excitation wavelength is changed, but the wavelength of the maximum emission band remains identical (λ_{emi} = 344 nm). This indicates the possible formation of relatively monodispersed sub-nanometer clusters, made by no more than 3–4 gold atoms.[29,34] These species could be formed by disaggregation from the larger extreme of ellipsoidal NPs, either by the media conditions or by possible collisions between particles after 45–90 seconds of reaction. Similar gold clusters were found in benzene/AOT RMs and the explanation given for this fact was the poor material exchange among droplets because of the unfavourable droplet–droplet interaction.[29] According to the results shown in the literature, clusters are preferably formed in a kinetically controlled process with low reaction rates, such as those provided by microemulsion techniques.[11,35] However, not all RMs show the same behavior, as it was demonstrated in previous results with AOT.[29]

The photoluminescence phenomenon observed take place in a narrow size scale of gold clusters due to the presence of band gaps in the atomic solid-state structure;[35] this is not the case for larger NPs when the band gap between the valence and conduction bands is insufficient to measure this fluorescence, because the gold particles show a size-dependent optical limiting effect in the range 2.5–15 nm.[36] Thus, the size reduction of the NPs to a few nanometers allows discrete energy levels to become accessible, and fluorescence phenomena take place.[35]

Our results suggest that these species are monodisperse because of the occurrence of a single narrow emission peak in the fluorescence spectra. As is well known, the atomic clusters are the building blocks of the nanoparticles and the pass through this stage before the nanoscale is extremely fast; the challenge is to get these sub-nanometer species as a product in the final stage of reaction. Nevertheless, more experiments are necessary to obtain detailed information such as the size, the structure, and properties. In any case, this is a very promising result taking into account the simplicity of the synthetic method in comparison with conventional top-down methodologies. In conclusion, by using BHDC RMs at W_0 = 6 it is possible to obtain two kinds of species that coexist: pseudo-elliptical AuNPs and sub-nanometer gold clusters.

The situation is different when the W_0 value is changed. Fig. 5 shows the kinetic formation of the AuNPs LSPR for the NPs synthesized in BHDC RMs at W_0 = 3.

As can be seen in Fig. 5A, the LSPR shows a single band whose intensity remains constant after 90 seconds of reaction. The position of the absorption maximum at 534 nm suggests a smaller size for the AuNPs as compared with those synthesized at W_0 = 6. All the LSPR spectra have a single absorption maximum; although the clear asymmetry in all cases suggests that NPs are not spherically-shaped.[30,31] As can be seen in Fig. 5B, the AuNPs obtained in these BHDC RMs are effectively smaller (17 ± 2 nm) than the AuNPs obtained at W_0 = 6. Also, as shown in the zoom-inset of Fig. 5B, they have different morphologies such as spheres, triangles and non-defined shapes (pseudo geometries), this micrograph suggests that the broad LSPR spectra also could be a product of the inter-particle coupling effect because of the proximity among NPs.[37] It is important to note that no fluorescence emission was obtained from samples synthesized at W_0 = 3, suggesting the absence of sub-nanometer gold particles. All of these phenomena could be explained by taking into account the following: in this system, BHDC molecules act as excellent stabilizing agents, supporting the NPs in solution, and preventing the aggregation and uncontrolled growth; it is clear to note that AuNPs are in the form of ''islands'' but each nanoparticle is independent of the others. On the other hand, in extremely pure media the shape of the small clusters can be retained as they grow to mesoscopic and even macroscopic scales. However, the presence of impurities such as ions can change the shape of the developing crystals by adsorption on selective sites.[12] As can be seen in Fig. 1, the BHDC surfactant has Cl^- as a counterion that can affect the development of initial facets of the crystal, favouring the anisotropic development of NPs with a broad multicomponent size distribution (Fig. 5C).[12,38,39] Considering that at W_0 = 3 the RMs are smaller in comparison with W_0 = 6, the anisotropic effect should be more important due to the proximity of gold precursors (involved in nucleation processes) to the interfacial zone where the Cl^- ions are present. Moreover, at W_0 = 3 the interface is less fluid than at W_0 = 6 and the inter-droplet interactions leading to dimer formation (RM–RM collisional interactions) are stiffer, resulting in smaller AuNPs. In this sense, it can be argued that the smaller size and rigidity of W_0 = 3 RM

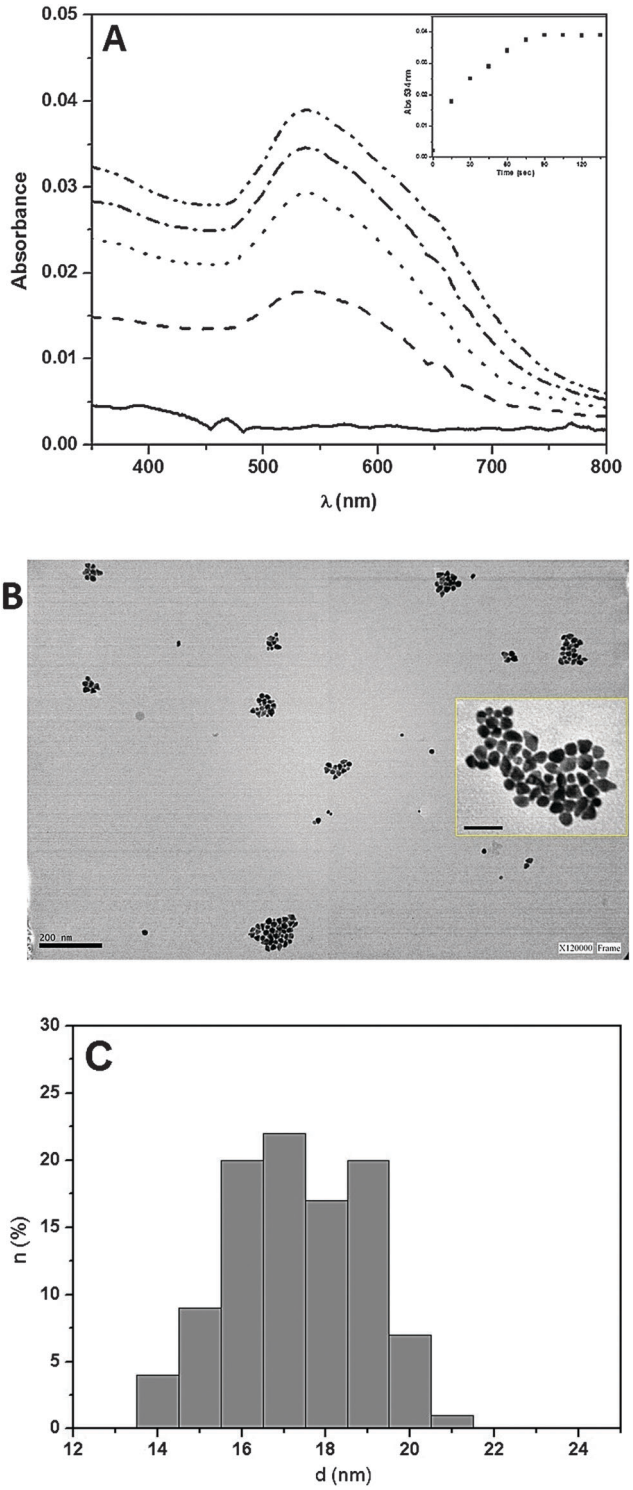

Fig. 5 (A) Absorption spectra of AuNP formation in toluene/BHDC/water at W_0 = 3. Time (s) = 0 (—), 15 (- - -), 45 (●●●), 60 (-·-) and 90 (–●●–). The inset in the top-right corresponds to the absorbance at λ = 534 nm *vs.* time (s). Aqueous BHDC RM solution (without precursors) was used as blank. (B) TEM micrographs of AuNPs synthesized in toluene/BHDC/water RMs at the end of the reaction (90 s). [BHDC] = 0.05 M, [$HAuCl_4$] = 0.005 M, [H_4N_2] = 0.3 M, W_0 = 3. Reference bar = 200 nm. The inset on the right side corresponds to a zoom of several AuNPs, and the reference bar to 50 nm, and (C) size distribution by number at the end of the reaction (90 s).

interfaces preclude the effective interaction between micelles in comparison with W_0 = 6 and a kind of ''island'' of NPs can be formed. These results are very attractive because anisotropic NPs have different electronic density areas that drastically affect their properties.[40] Indeed, metal NPs with well-defined non-spherical morphologies are very promising dual functional nanomaterials, with capabilities of simultaneously serving as near infrared-activatable photodynamic and photothermal therapy reagents for cancer treatments.[41,42]

AuNPs in toluene:hexane (X_{Hx} = 0.25)/BHDC/water RMs

The effect of the external organic media composition on the AuNPs synthesis was studied using a toluene:hexane blend. It is important to note that, as was reported before,[22,28] when the aliphatic content increases in aromatic:aliphatic blends, the W_0 maximum of BHDC RMs decreases. Taking into account these facts, we choose the molar fraction X_{Hx} = 0.25 in order to prepare stable BHDC RMs at W_0 = 3 and 6, and to compare with toluene/BHDC systems at both W_0. Under these conditions (X_{Hx} = 0.25) the d_{app} of the nanoreactors was 10.5 ± 0.5 nm at W_0 = 6 and 6 ± 0.5 nm at W_0 = 3. The diameters of the BHDC RMs could suggest that the micellar interactions were enhanced, d_{app} in the aromatic:aliphatic blend being almost twice as large in comparison with the pure aromatic system.[29] This may be because interactions between the surfactant and the external non-polar solvent in the blend are stronger than in the pure aromatic solvent.[23] Herein, this system is quite interesting because the changes in their interactions may have an important impact on the metal reduction process.

Fig. 6 shows the absorption spectra evolution of AuNPs synthesized in toluene:hexane/BHDC/water at W_0 = 6.

As can be observed in Fig. 6A, the evolution of LSPR is very different in comparison with toluene/BHDC (Fig. 3A); here a unique Gaussian absorption band at λ = 528 nm is observed, which experiences a hypsochromic shift until λ = 521 nm with time and remains constant after 90 seconds of reaction. The electron micrograph and the size distribution obtained for the final product by TEM and DLS (Fig. 6B and C) show spherical AuNPs with diameters of around 11 ± 2 nm and narrow component distribution characteristic for monodisperse particles in colloidal systems. It is very interesting to find how with a small addition of an aliphatic solvent to the external organic phase, the concentration, morphology, optical properties and the size of the AuNPs were modified. With only 15 seconds of reaction it is possible to observe a complete Gaussian absorption band. This impact of aliphatic solvent can be explained by taking into account the enhanced droplet–droplet interactions and the canal expansion due to higher interface flexibility.[18,29] Both phenomena favor the reactant interchange between droplets and improve the rate of the nucleation process; this can be seen in the large monodispersity and smaller size of AuNPs synthesized under these conditions (Fig. 6B and C) in comparison with toluene/BHDC RMs (Fig. 3B and C). These results agree with previous work where *n*-heptane/AOT and benzene/AOT were studied in gold nanoparticle synthesis.[18,29]

The situation observed in toluene:hexane/BHDC/water RMs is quite different at W_0 = 3.

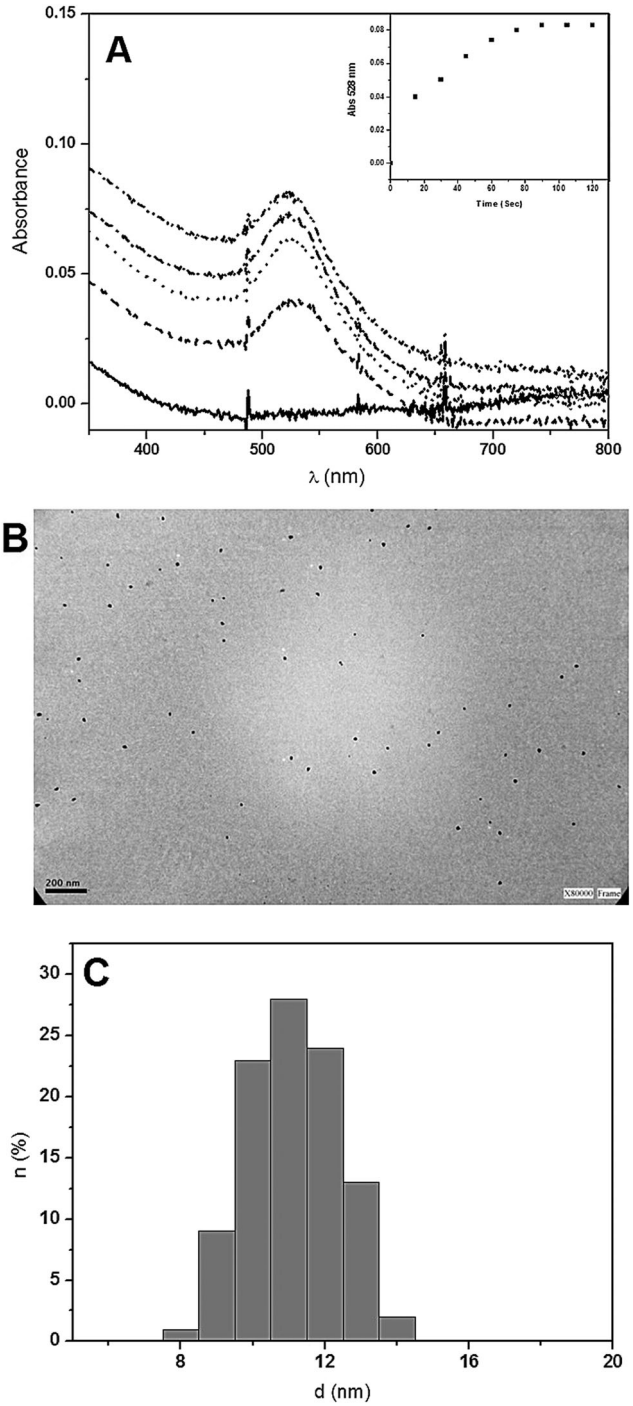

Fig. 6 (A) Absorption spectra of AuNP formation in toluene:hexane (X_{Hx} = 0.25)/BHDC/water at W_0 = 6. Time (s) = 0 (—), 15 (- - -), 45 (●●●), 60 (-··-) and 90 (–●●–). The inset in the top-right corresponds to the absorbance at λ = 528 nm *vs.* time (s). Aqueous BHDC RM solution (without precursors) was used as blank. (B) TEM micrographs of AuNPs synthesized in toluene:hexane (X_{Hx} = 0.25)/BHDC/water RMs at the end of the reaction (90 s). [BHDC] = 0.05 M, [$HAuCl_4$] = 0.005 M, [H_4N_2] = 0.3 M, W_0 = 6. Reference bar = 200 nm, and (C) size distribution by number at the end of the reaction (90 s).

Fig. 7 shows the absorption spectra obtained for toluene:hexane (X_{Hx} = 0.25)/BHDC/water RMs at W_0 = 3. Here, the LSPR shows a single band whose intensity remains constant after

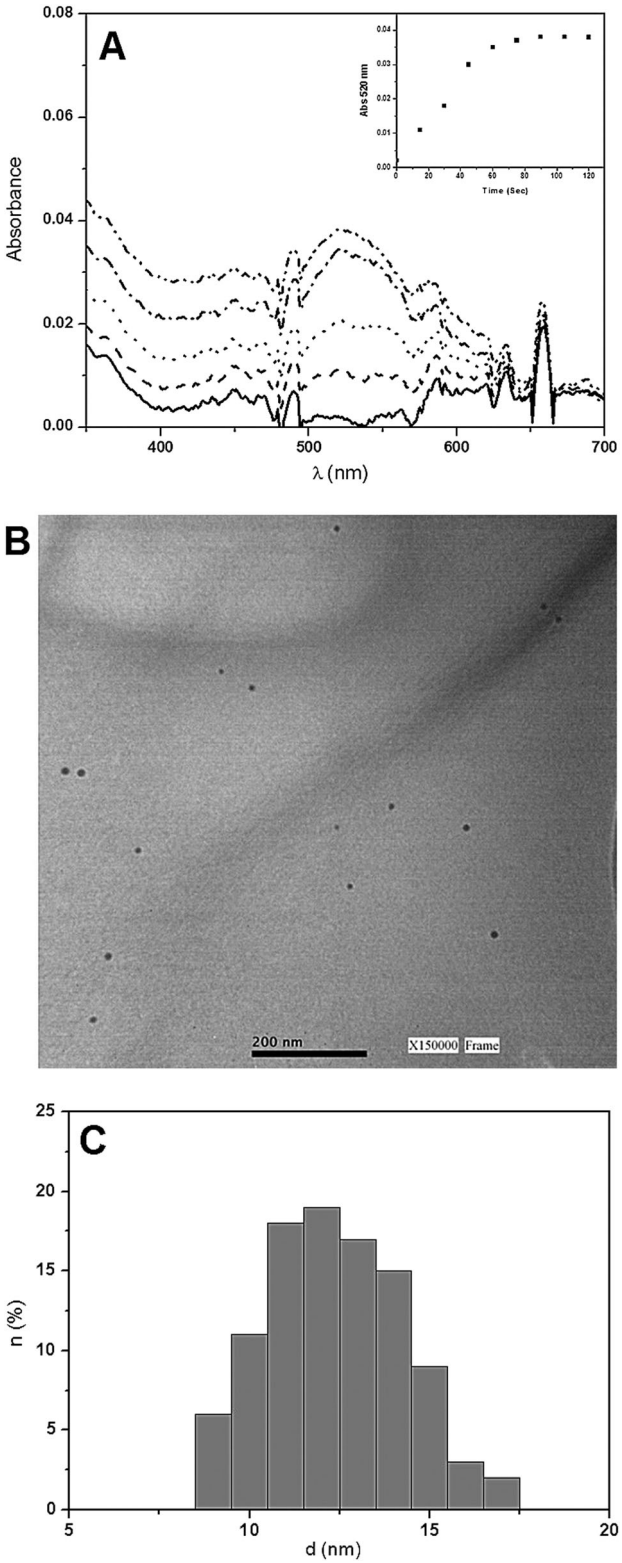

Fig. 7 (A) Absorption spectra of AuNP formation in toluene:hexane (X_{Hx} = 0.25)/BHDC/water at W_0 = 3. Time (s) = 0 (—), 15 (- - -), 45 (●●●), 60 (-·-) and 90 (–●●–). The inset on the top-right corresponds to the absorbance at λ = 521 nm *vs.* time (s). Aqueous BHDC RM solution (without precursors) was used as blank. (B) TEM micrographs of AuNPs synthesized in toluene:hexane (X_{Hx} = 0.25)/BHDC/water RMs at the end of the reaction (90 s). [BHDC] = 0.05 M, [$HAuCl_4$] = 0.005 M, [H_4N_2] = 0.3 M, W_0 = 3. Reference bar = 200 nm, and (C) size distribution by number at the end of the reaction (90 s).

80 seconds of reaction. The position of the absorption maximum at 520 nm suggests smaller AuNPs than those obtained at the same W_0 in pure toluene/BHDC (Fig. 5). This is supported with the TEM micrographs and size distributions by DLS (Fig. 7B and C), where diameters of around 13 nm and a multicomponent distribution in this size range were found; unfortunately the concentration of NPs is lower than in the system at W_0 = 6 and the poor intensity of the absorption spectra is affected by lamp issues from the UV equipment showing some ''peaks'' on the baseline. This shows how a small hexane addition to the external organic phase allows us to modify the nanoparticle size and shape, due to the better droplet–droplet interaction, more extended ''exchange channel'' (Fig. 2) and consequently better reactant interchange. Thus, if we compare the BHDC RMs as nanoreactors in pure toluene with toluene:hexane (X_{Hx} = 0.25), it is clear how the aliphatic solvent favors the reaction process. In this way, two important facts can be highlighted: (A) the polar core size is crucial for the anisotropy of nanoparticles due to the insertion of Cl^- counterions of BHDC in the earlier crystalline layers inducing morphological changes. (B) The effectiveness of intermicellar interaction and the reduction process increases with hexane addition, reducing the final size and polydispersity of the AuNPs. These two phenomena can be explained as follows: the shape control of crystals is given by the Gibbs–Curie–Wulff theorem.[43] In the Wulff construction,[44] each facet of the crystal is described by its free surface and interfacial energies, and the crystal shape results from minimizing these energies for a certain volume.[12] Several years later, a newly proposed pseudo Wulff construction[45] was based on the fact that the driving factor was the growth rate of each facet instead of the equilibrium surface, suggesting that this is determined by kinetic control. Hence, the nucleation stage for the growth of anisotropic shapes plays a key role in determining the size/shape of the resulting nanocrystals.[12] In this way, the AuNPs synthesized by the soft chemistry methodology used in this study are governed by kinetic phenomena, therefore it makes sense to obtain anisotropic species in the toluene/BHDC/water, when the micelle–micelle interactions are less effective than in toluene:hexane/BHDC/water, when the hexane molecules favor the precursor interchange and the reduction effectiveness, decreasing Cl^- insertions in the first stage of the gold crystals.

Since our results show that the BHDC RMs have smaller diameters than the NPs obtained, we think that once the metal particles are formed, the micelles stop acting as molecular assemblies and the surfactant molecules begin to act as stabilizing agents, capping the nanoparticles not necessarily as a ''big'' reverse micelle. Hence, RMs are not essentially nanotemplates of metal NPs as is commonly thought, showing here that each system is a unique nanoreactor. In this way, note that these results are very different in comparison with ternary AOT RMs (non-polar solvent/AOT/precursors in water), where the nanoparticles obtained are always spherical.[9,29] This may be due to the effectiveness of micelle–micelle interactions and mainly due to the unusual properties of water molecules at the interface in both systems. Previous studies by our group showed differences in water entrapped in both systems using emission and absorption

spectroscopies and molecular probes such as hemicyanine *trans*-4-[4-(dimethylamino)-styryl]-*N*-methylpyridinium iodide and the complex *N*,*N*,*N*,*N*′-tetramethylethylenediamine copper(II).[27,45] Thus, the water dissolved by BHDC RMs is unable to act as an electron donor because the non-bonding electron pairs of water's oxygen are completely involved in the cationic BHDC polar head group solvation through an ion–dipole interaction. In contrast, in AOT RMs the water molecules solvate the sulfonate group through hydrogen bonding interactions, as a consequence the bulk hydrogen bond network is destroyed at the interface and therefore, the electron pairs are more available to interact with the microenvironment.[27,46] Thus, the electron donor ability of the entrapped water can be significantly altered depending on the kind of surfactant used to prepare the RMs.[27,45] Moreover, when these RMs were used as nanoreactors, for example in the hydrolysis of 2-naphthyl acetate catalyzed by the enzyme α-chymotrypsin (α-CT) in benzene/BHDC/water RMs and its efficiency was compared with that observed in pure water and in AOT RMs, the results show that the catalytic efficiency obtained in RM systems are higher than the value reported in water.[47] Furthermore, there is a remarkable increase in the α-CT efficiency in the cationic BHDC RMs in comparison with the anionic AOT system, believably due to the unique water properties found in these confined media. Particularly, these results demonstrated that in cationic RMs the hydrogen-bond donor capacity of water is enhanced due to its interaction with the cationic interface. Hence, entrapped water can be converted into ''super-water'' for enzymatic reactions studied in confined environments.

In this sense, the unusual water properties provided by the BHDC RMs may have a high impact on NPs synthesis because the precursors will be more exposed to interact inside the RMs.

Conclusion

In this work, we demonstrate that it is possible to get different types of nanostructures inside cationic reverse micelles by changing the quantity of water dissolved or the external solvent composition, which may have a strong impact on nanotechnology. Thus, using reverse micelles as nanoreactors, not only gold nanoparticles are stable and in equilibrium with different morphologies, but also sub-nanometer species. Because these tiny particles and anisotropic nanoparticles are found to be very active in many applications, this simple synthetic method can be of high importance in many applications nowadays. Additionally, the results of this work show the importance of understanding the behavior of reverse micelles in order to apply them in a specific field, because just by small changes in their composition it is possible to obtain different nanocomposites.

Experimental

Materials

Toluene and hexane both of HPLC grade were purchased from Sigma and were used without further purification. Benzyl-*n*-hexadecyldimethylammonium chloride (BHDC) (Sigma >99% purity) was used as received, and to minimize water absorption, it was kept under vacuum over P_2O_5. Ultrapure water was obtained using Labonco equipment model 90901-01. Tetrachloroauric acid ($HAuCl_4$, Sigma-Aldrich) as a precursor and hydrazine (N_2H_4, Sigma-Aldrich) as a reducing agent, both for the synthesis of gold nanoparticles were used as received.

Methods

The stock solutions of BHDC RMs in toluene or a toluene: hexane blend were prepared by mass and volumetric dilution. To obtain optically clear solutions, they were shaken in a sonicating bath and water was added using a calibrated microsyringe. The amount of water present in the system is expressed as the molar ratio between the polar solvent and the surfactant, W_0 = [water]/[BHDC]. All experimental points were measured three times with different prepared samples. The pooled standard deviation was less than 5%. In all cases, the temperature was maintained at 25 °C ± 0.2 °C.

The methodology used to synthesize AuNPs in RMs is described by Lopez-Quintela,[11] where the reactants (tetrachloroauric acid and hydrazine) interact and the auric ions are reduced for nucleation and growth in a limited space (polar core). For example, a solution of toluene (or toluene:hexane)/BHDC RMs containing tetrachloroauric acid dissolved at [BHDC] = 0.05 M and W_0 = 6, and another containing hydrazine dissolved in BHDC RMs at the same BHDC concentration and W_0 = 6 were prepared. The reduction process takes place when the two BHDC RM systems are mixed by magnetic agitation at room temperature. The same procedure was performed for the BHDC RMs at W_0 = 3. The concentration of precursors based on the volume of aqueous solution was kept constant in all systems, $[HAuCl_4]$ = 0.005 M, $[H_4N_2]$ = 0.3 M.

General

UV/visible spectra were recorded using a Hewlett Packard-Agilent 8453 spectrophotometer with a thermostated sample holder. Spex fluoromax apparatus was employed for the fluorescence measurements. Corrected fluorescence spectra were obtained using the correction file provided by the manufacturer. The path length used in all experiments was 1 cm.

All the DLS experiments were carried out at a fixed BHDC concentration of 0.05 M. Hence, the RM solutions are not at infinite dilution, thus, we considered it appropriate to introduce an apparent hydrodynamic diameter (d_{app}) in order to make a comparison of our systems as it was used before.[2,22] The apparent hydrodynamic diameters of different BHDC RMs were determined by dynamic light scattering (DLS, Malvern 4700 with goniometer) with an argon-ion laser operating at 488 nm. BHDC RM samples were filtered using an Acrodisc with a 0.2 μm polytetrafluoroethylene (PTFE) membrane (Sigma). For DLS analyses, the viscosities and refractive indices of the solvent blends are required; the viscosities of the toluene:hexane systems were taken from the literature.[48,49] The refractive indices of the solvent mixtures were calculated by using the first-order approximation shown in eqn (1), $\eta D1$ and $\eta D2$ are the pure solvent refractive indices.

$$\eta D = X1\eta D1 + X2\eta D2 \quad (1)$$

The effect of temperature on ηD of these solvents was small enough to be ignored. This approximation gives good and reliable results.[47] Thirty independent size measurements were made for each individual sample at the scattering angle of 90°; the polydispersity indices of the experiments were always below 0.2. The algorithm used was CONTIN. The apparent hydrodynamic diameter values reported were weighted by intensity, volume, and/or number as no differences were observed. The DLS experiments show that the polydispersity of the BHDC RM size is less than 5%. Under our experimental conditions, we obtained a resolution of 0.5 nm.

The micrographs were recorded using a JEOL JEM EXII 1200 Transmission Electron Microscope at 80 kV with a Gatan ES100W camera and Gatan Digital Micrograph software. For TEM studies, the RM samples were placed into a formvar-covered copper grid and evaporated slowly.

Acknowledgements

We gratefully acknowledge financial support for this work by the Consejo Nacional de Investigaciones Científicas y Técnicas (CONICET), Agencia Nacional de Promoción Científica y Técnica and Secretaría de Ciencia y Técnica of the Universidad Nacional de Río Cuarto. J.J.S., N.M.C. and R.D.F. hold research positions at CONICET. J.A.G and M.A.L. thank CONICET for research fellowships.

References

1 S. K. Yadav, Z. A. Khan and B. Mishra, *Rev. Nanosci. Nanotechnol.*, 2013, **2**, 127–142.
2 O. V. Salata, *Nanobiotechnology*, 2004, **2**, 1–6.
3 M. C. Daniel and D. Astruc, *Chem. Rev.*, 2004, **104**, 293–346.
4 P. C. Chen, S. C. Mwakwari and A. K. Oyelere, *Nanotechnol., Sci. Appl.*, 2008, **1**, 45–65.
5 P. K. Jain, X. Huang, I. H. El-Sayed and M. A. El-Sayed, *Acc. Chem. Res.*, 2008, **41**, 1578–1586.
6 R. Hong, G. Han, J. M. Fernández, B. J. Kim, N. S. Forbes and V. M. Rotello, *J. Am. Chem. Soc.*, 2006, **128**, 1078–1079.
7 G. Han, C. C. You, B. J. Kim, R. S. Turingan, N. S. Forbes, C. T. Martin and V. M. Rotello, *Angew. Chem., Int. Ed.*, 2006, **45**, 3165–3169.
8 E. E. Connor, J. Mwamuka, A. Gole, C. J. Murphy and M. D. Wyatt, *Small*, 2005, **1**, 325–327.
9 A. B. Smetana, J. S. Wang, J. Boeckl, G. J. Brown and C. M. Wai, *Langmuir*, 2007, **23**, 10429–10432.
10 C. Tojo, M. C. Blanco and M. A. Lopez-Quintela, *Langmuir*, 1998, **14**, 6835–6839.
11 M. A. Lopez-Quintela, *Curr. Opin. Colloid Interface Sci.*, 2003, **8**, 137–144.
12 M. P. Pileni, *J. Phys. Chem. C*, 2007, **111**, 9019–9038.
13 N. M. Correa, J. J. Silber, R. E. Riter and N. E. Levinger, *Chem. Rev.*, 2012, **12**, 4569–4602.
14 D. Myers, *Surfactant Science and Technology*, John Wiley and Sons, New Jersey, 3rd edn, 2006.
15 M. J. Hou, M. Kim and D. O. Shah, *J. Colloid Interface Sci.*, 1988, **123**, 398–412.
16 A. M. Cazabat and D. Langevin, *J. Chem. Phys.*, 1981, **74**, 3148–3158.
17 B. Lemaire, P. Bothorel and D. Roux, *J. Phys. Chem.*, 1983, **87**, 1023–1028.
18 F. M. Agazzi, N. M. Correa and J. Rodriguez, *Langmuir*, 2014, **30**, 9643–9653.
19 A. Salabat, J. Eastoe, K. J. Mutch and R. F. Tabor, *J. Colloid Interface Sci.*, 2008, **318**, 244–251.
20 O. Myakonkaya, J. Eastoe, K. J. Mutch, S. Rogers, R. Heenan and I. Grillo, *Langmuir*, 2009, **25**, 2743–2748.
21 M. J. Hollamby, R. Tabo, K. J. Mutch, K. Trickett, J. Eastoe, R. Heenan and I. Grillo, *Langmuir*, 2008, **24**, 12235–12240.
22 F. Agazzi, R. D. Falcone, J. J. Silber and N. M. Correa, *J. Phys. Chem. B*, 2011, **115**, 12076–12084.
23 F. M. Agazzi, J. Rodriguez, R. D. Falcone, J. J. Silber and N. M. Correa, *Langmuir*, 2013, **29**, 3556–3566.
24 D. Mandal, A. Datta, P. S. Kumar and K. Bhattacharyya, *J. Phys. Chem. B*, 1998, **102**, 9070–9073.
25 M. Harada, K. Saijo, N. Sakamoto and K. Ito, *J. Colloid Interface Sci.*, 2010, **343**, 423–432.
26 H. Lu, H. Ju, Q. Yang, Z. Li, H. Ren, X. Xin and G. Xu, *CrystEngComm*, 2013, **15**, 6511–6517.
27 D. Blach, N. M. Correa, J. J. Silber and R. D. Falcone, *J. Colloid Interface Sci.*, 2011, **355**, 124–130.
28 J. S. F. Tabares, N. M. Correa, J. J. Silber, L. E. Sereno and P. G. Molina, *Soft Matter*, 2015, **11**, 2952–2962.
29 J. A. Gutierrez, R. D. Falcone, M. A. Lopez-Quintela, D. Buceta, J. J. Silber and N. M. Correa, *Eur. J. Inorg. Chem.*, 2014, 2095–2102.
30 D. E. Mustafa, T. Yang, Z. Xuan, S. Chen, H. Tu and A. Zhang, *Plasmonics*, 2010, **5**, 221–231.
31 K. L. Kelly, E. Coronado, L. L. Zhao and G. C. Schatz, *J. Phys. Chem. B*, 2002, **107**, 668–677.
32 K. Kumar Dey, A. Kumar, R. Shanker, A. Dhawan, M. Wan, R. Ram Yadavc and A. Kumar Srivastava, *RSC Adv.*, 2012, **2**, 1387–1403.
33 R. Vankayala, C. L. Kuo, A. Sagadevan, P. H. Chen, C. S. Chiang and K. C. Hwang, *J. Mater. Chem. B*, 2013, **1**, 4379–4387.
34 B. S. González, M. J. Rodriguez, C. Blanco, J. Rivas, M. A. López-Quintela and J. M. G. Martinho, *Nano Lett.*, 2010, **10**, 4217–4221.
35 C. Vazquez-Vazquez, M. Bañobre-Lopez, A. Mitra, M. A. López-Quintela and J. Rivas, *Langmuir*, 2009, **25**, 8208–8216.
36 (*a*) A. W. Snow and H. Wohltjen, *Chem. Mater.*, 1998, **10**, 947–949; (*b*) L. François, M. Mostafavi, J. Belloni, J.-F. Delouis, J. Delaire and P. Feneyrou, *J. Phys. Chem. B*, 2000, **104**, 6133–6137.
37 S. Kumar Ghosh and T. Pal, *Chem. Rev.*, 2007, **107**, 4797–4862.
38 T. H. Tran and T. D. Nguyen, *Colloids Surf., B*, 2011, **88**, 1–22.
39 I. Lisiecki, *J. Phys. Chem. B*, 2005, **109**, 12231–12244.

40 R. Narayan and M. A. El-Sayed, *J. Am. Chem. Soc.*, 2004, **126**, 7194–7195.
41 R. Vankayala, C. L. Kuo, A. Sagadevan, P. H. Chen, C. S. Chiang and K. C. Hwang, *J. Mater. Chem. B*, 2013, **1**, 4379–4387.
42 A. Corma, P. Concepción, M. Boronat, M. J. Sabater, J. Navas, M. J. Yacaman, E. Larios, A. Posadas, M. A. López-Quintela, D. Buceta, E. Mendoza, G. Guilera and A. Mayoral, *Nat. Chem.*, 2013, **5**, 775–781.
43 J. W. Mullin, *Crystallization*, Butterworth Heinemann, Boston, 4th edn, 2001.
44 G. Z. Wulff, *Kristallografiya*, 1901, **34**, 449–513.
45 J. Buhler and Y. Prior, *J. Cryst. Growth*, 2000, **209**, 779–788.
46 S. S. Quintana, F. Moyano, R. D. Falcone, J. J. Silber and N. M. Correa, *J. Phys. Chem. B*, 2009, **113**, 6718–6724.
47 F. Moyano, R. D. Falcone, J. C. Mejuto, J. J. Silber and N. M. Correa, *Chem. – Eur. J.*, 2010, **16**, 8887–8893.
48 H. Iloukhani, M. R. Sameti and J. B. Parsa, *J. Chem. Thermodyn.*, 2006, **38**, 975–982.
49 N. Calvar, E. Gómez, B. González and Á. Domínguez, *J. Chem. Thermodyn.*, 2009, **41**, 939–944.